Photo-oxidation pathway as a potential CS_2 sink in the atmosphere

Y. Li[1] , K. Kazuki[2] , and S.O. Danielache[1]

[1]Department of Material and Life Science, Faculty of Science and Technology, Sophia University, Tokyo, Japan

[2]National Institute of Advanced Industrial Science and Technology, Japan

Corresponding author: Yuanzhe Li (liyuanzhe@eagle.sophia.ac.jp)

Key Points:

- A sulfur cycle with the addition of the carbon disulfide photo-oxidation pathway was implemented and tested by a 1-dimensional model.
- The photo-oxidation pathway accounts for up to 15.8% of carbon disulfide atmospheric chemical removal in the global average.

Abstract:

A 1D model of the CS_2 reaction network with the addition of the photo-oxidation pathway has been developed. The sulfur flux analysis was applied to determine the importance of the photo-oxidation pathway in the atmospheric CS_2 sink, 15.8% of sulfur flux passes through the photo-oxidation pathway under the global average solar radiation conditions and ranging from 8.1% to 18% depending on the local irradiance intensity. The concentration of COS and SO_2, the main products of CS_2 atmospheric oxidation, changed slightly from the sulfur cycle developed with the updated CS_2 reaction network. 5% of the COS comes from the new pathway and a total of 47% of COS comes from the conversion of CS_2. The sulfur budget for the main species in the sulfur cycle is constructed and the CS_2 lifetime is estimated as 2-3 days. The newly added photo-oxidation pathway plays an important role in the CS_2 reaction network and has a high variability under specific geochemical conditions.

1 Introduction

Carbon disulfide (CS_2) is a common atmospheric trace gas mainly distributed in the troposphere. The oxidation of CS_2 accounts for 30-75% of the global carbonyl sulfide (COS) budget [*Chin and Davis*, 1993; *Khalil and Rasmussen*, 1984; *Toon et al.*, 1987; *Whelan et al.*, 2018]. COS has a long lifetime (> 1 year) [*Mopper et al.*, 2015], and it can transport to the upper atmosphere and produce stratospheric sulfur aerosol (SSA) [*Crutzen*, 1976; *Weisenstein et al.*, 1997], which is important for shielding radiation and regulating global temperature. CS_2 also produces sulfur dioxide (SO_2), and it directly participates in the formation of acid rain [*Sze and Ko*, 1980], harming plants and animals [*Hajer*, 2002]. Anthropogenic sources account for 60% of total CS_2 emissions [*Chin and Davis*, 1993], mainly from industrial production and transportation [*C-L Lee and Brimblecombe*, 2016], and has a year-on-year trend of increasing [*Bandy et al.*, 1981; *Khalil and Rasmussen*, 1984; *Weisenstein et al.*, 1997]. Therefore, the impact of CS_2 on the environment cannot be ignored.

CS_2 is mainly depleted in the lower atmosphere and is hardly detected at 5-6 km, suggesting the ground-based sources and rapid atmospheric removal [*Bandy et al.*, 1981]. Current understanding expounds that the main CS_2 sink is through the oxidation with OH radicals to produce COS and SO_2 as the end-oxidized products [*Khalil and Rasmussen*, 1984]. A previous model study suggests OH-oxidation pathway shares 75-88% of CS_2 global removal [*Khan et al.*, 2017]. In addition, the calculated residence time in the atmosphere is from a few days to half of a month, varying according to the extent of pollution and human activities [*Khalil and Rasmussen*, 1984].

The UV absorption spectrum of CS_2 shows two distinct highly structured bands [*Burkholder et al.*, 2020]. The strong absorption band extending from 185-230 nm denotes the CS_2 photolysis reaction and is included in some CS_2 model studies [*Khan et al.*, 2017; *Kjellström*, 1998; *Weisenstein et al.*, 1997]. However, due to the strong absorption by air gases such as oxygen and ozone, the UV light with wavelength shorter than 320 nm can hardly reach the surface, resulting in the CS_2 photolysis reaction barely occurring in the troposphere. Meanwhile, the weaker band extending from 290-380 nm excites the CS_2 molecule (the excited state is expressed as CS_2^* in this study) and triggers a photo-oxidation pathway, producing the same products as the OH-oxidation pathway through a series of oxidation reactions [*Wood and*

Heicklen, 1971]. Although the CS_2 absorption band that triggers the photolysis reaction are three orders of magnitude larger than the cross-sections of the photo-excitation reaction [*Grosch et al.*, 2015], CS_2 can hardly reach the upper atmosphere, resulting in the CS_2 photolysis being irrelevant in the atmospheric sulfur cycle, consequently CS_2 photochemistry has been neglected in the previous sulfur cycle model studies [*Brühl et al.*, 2011; *Kremser et al.*, 2016; *Mills et al.*, 2017; *Sheng et al.*, 2015; *Weisenstein et al.*, 1997]. The solar radiation at different altitudes was calculated using a 1D chemical transport model PATMO (Planetary ATMOSpheres) [*Danielache et al.*, 2023], which compares favorably with reference data [*Kerr and Fioletov*, 2008]. **Figure 1** shows that the atmospheric absorption is very weak for irradiance with wavelengths longer than 320 nm, indicating the long wavelength solar radiation can reach the ground and provide enough photons for the CS_2 photo-excitation reaction to occur in the lower atmosphere. Several studies have been conducted to detect the fluorescence of CS_2 under long wavelength radiation [*Brus*, 1971; *Lambert and Kimbell*, 1973] and the photo-oxidation pathway was elaborated as a potential atmospheric COS source [*Lambert and Kimbell*, 1973]. However, there are no quantitative studies to elucidate the role of new reaction pathways in the reaction network of CS_2 and the contribution to atmospheric COS.

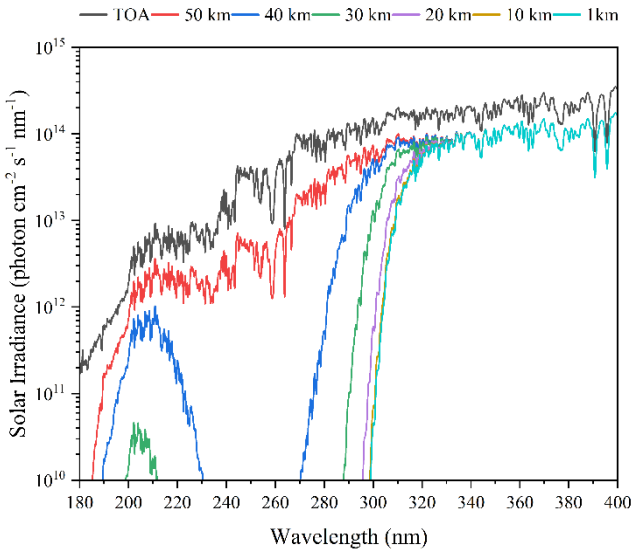

Figure 1. Solar irradiance at different altitudes using the opacity values calculated from the PATMO (Planetary ATMOSphere). The daytime-weighted method is applied to counteract the spatial-temporal variation in the 1D model and to represent the global averaging solar irradiance level.

This study discusses the CS_2 reaction network and applies a sulfur flux analysis method to study the influence of the CS_2 photo-oxidation pathway on the atmospheric sulfur cycle. A revised atmospheric CS_2 reaction network with the addition of the photo-oxidation pathway is introduced and tested in a 1D model PATMO.

2 Model Description

The chemistry of atmospheric CS_2 has been incorporated into the 1D chemical transport model PATMO, which has been proven reliable for atmospheric chemistry simulation [*Avila et al.*, 2021] and is designed to handle photochemistry with high-resolution absorption spectra [*Danielache et al.*, 2023]. The model calculates photodissociation and photo-excitation rate constants at each layer. The altitude-dependent rate constants are calculated by correcting for the solar flux changes caused by the absorption of photosensitive species upon the solar flux entering the atmosphere. Details of the photochemical calculation in the model can be found in the work of *Danielache et al.* [2023].

To compensate for the 1D model's common inability to account for spatial-temporal variation, we choose the daytime-weighted method by setting the zenith angle θ at 60° and solar constant $I(\infty,\lambda)$ at half to counteract the cyclical fluctuations of solar flux from annual cycle and diurnal cycle. More studies on radiative-convective equilibrium [*Manabe and Strickler*, 1964; *Manabe and Wetherald*, 1967; *Ramanathan*, 1976], the exoplanetary climate [*Wordsworth et al.*, 2010], and the estimates of the global radiative forcing caused by aerosols and clouds [*Fu and Liou*, 1993; *L. Zhang et al.*, 2013] showed that the agreements on using the daytime-weighted adjustment to reduce the solar radiation bias in the 1D model simulation. The cross-section of Rayleigh scattering to air in the UV band is less than one-thousandth of the cross-section of photochemical reactions in the model [*Bates*, 1984; *He et al.*, 2021; *Thalman et al.*, 2014]. Meanwhile, atmospheric gas molecules are too small for the Mie scattering induced by solar radiation in the atmosphere [*Seinfeld and Pandis*, 2006], and aerosols are not the focus of this study. Therefore, light scattering by molecules and aerosols is not included. Only the direct solar radiation attenuated by the absorption of photochemically relevant molecules at each layer is considered for light intensity calculation.

Table 1. Emission rates and deposition velocities of the sulfur compounds.

Species	Emission (Tg $year^{-1}$)	Dry deposition (cm s^{-1})	Henry's constant (M atm^{-1})
COS	1.3	9.5×10^{-3}	0.02
CS_2	1.2	4.48×10^{-2}	0.05
SO_2	105.4	1	4000
H_2S	7.72	1.7×10^{-1}	0.1
DMS	65.57	1.48×10^{-1}	——
SSA	——	——	5×10^{4}

Note. **Emission rates [*C-L Lee and Brimblecombe*, 2016; *Watts*, 2000; *Zhong et al.*, 2020] and deposition velocities of CS_2 and its end-oxidation products COS and SO_2 [*Belviso et al.*, 2013; *Burkholder et al.*, 2020; *C-L Lee and Brimblecombe*, 2016; *Seinfeld and Pandis*, 2006] are prepared for CS_2 reaction network. Dry deposition of CS_2 and SO_2 is calculated from reference lifetime data [*Colman and Trogler*, 1997; *C Lee et al.*, 2011]. Emission rates [*C-L Lee and Brimblecombe*, 2016; *Watts*, 2000] and deposition velocities [*Cope and Spedding*, 1982; *Judeikis and Wren*, 1977] for H_2S and DMS are added for complete sulfur cycle calculation. The effective Henry's constant for SO_2 is suggested by *Giorgi and Chameides* [1985], and the rest uses recommended data from *Burkholder et al.* [2020].**

Emission processes are set as a continuous flux of CS_2, COS, and SO_2 species into the lowermost layer. The estimated global emission data are listed in **Table 1**, in teragrams per year units $(\mathrm{Tg\,year^{-1}})$ in the model, this data is converted to number density flux $(\mathrm{molecule\,cm^{-3}\,s^{-1}})$ following the expression:

$$E_{i(molecule\,cm^{-3}\,s^{-1})} = \frac{E_{i(Tg\,year^{-1})} \times (1 \times 10^{12})}{(3.154 \times 10^{7}) \times M_i} \times N_A/(V_B)$$

Where $E_{i(molecule\,cm^{-3}\,s^{-1})}$ is the emission of species i in the unit of $molecule\,cm^{-3}\,s^{-1}$; $E_{i(Tg\,year^{-1})}$is the emission of species i in the unit of $Tg\,year^{-1}$; the constant 1×10^{12} represents the unit conversion from Tg to g; the constant 3.154×10^{7} represents the unit conversion from year to second; M_i is the molar mass $(\mathrm{g\,mol^{-1}})$ of the species i; N_A is the Avogadro number; and V_B $(\mathrm{cm^3})$ is the volume of the boundary cell where the emission process happens, and it is approximated by:

$$V_B = \frac{4}{3} \times \pi \times (r_1^3 - r_2^3)$$

Where r_2 is the average radius of the Earth, which is approximated as $6.371 \times 10^{8}\,cm$, and considering the model cell is set as 1km in height, thus the r_1 equals to 6.372×10^{8} cm.

Dry deposition represents a range of material removal processes, including sedimentation, diffusion processes, or impact and interception due to turbulent transport [*Jacobson*, 2005; *Seinfeld and Pandis*, 2006]. The dry deposition flux F_d $(\mathrm{molecule\,cm^{-2}\,s^{-1}})$ is calculated based on the reported dry deposition velocity v_d $(\mathrm{cm\,s^{-1}})$ [*Belviso et al.*, 2013; *Burkholder et al.*, 2020; *Cope and Spedding*, 1982; *Judeikis and Wren*, 1977; *C-L Lee and Brimblecombe*, 2016; *Seinfeld and Pandis*, 2006] following the expression:

$$F_{d,i} = -v_{d,i} \times n_i$$

Where the number density n_i $(\mathrm{molecule\,cm^{-3}})$ of species i is approximated by the following expression under steady-state conditions [*Seinfeld and Pandis*, 2006]:

$$n_i = \tau_i \times P_i = \tau_i \times R_i$$

That τ_i (s) is the estimated lifetime of species i; and the rate of injection P_i $(\mathrm{molecule\,cm^{-3}\,s^{-1}})$ of the species i equals its rate of removal R_i $(\mathrm{molecule\,cm^{-3}\,s^{-1}})$ [*C-L Lee and Brimblecombe*, 2016; *Zhong et al.*, 2020].

Wet deposition is defined as natural processes by which the material is scavenged by atmospheric hydrometers and transported to the Earth's surface [*Seinfeld and Pandis*, 2006]. Considering that the amount of water in the atmosphere is too small above an altitude of 12 km and that the low temperature makes it in the form of ice, this means that the absorption process can be neglected, therefore the wet deposition process is restricted to take place below 12 km in the model. The effective Henry's law coefficients for SO_2 [*Giorgi and Chameides*, 1985], CS_2, and COS [*Burkholder et al.*, 2020] are listed in **Table 1**, and the wet deposition mechanism

follows the work of *Giorgi and Chameides* [1985].

This study focuses on the chemical transformation of sulfur species, and therefore the atmospheric profiles of common gases, which are N_2, O_2, O_3, OH, O, CO_2, CO, HO_2, H_2O, and NO_2, are set at the steady state conditions [*Hu et al.*, 2012; *Krueger and Minzner*, 1976; *Turco et al.*, 1979]. Environmental parameters such as temperature, pressure, and diffusion coefficient at each layer are all set as constant parameters [*Hu et al.*, 2012; *Krueger and Minzner*, 1976]. The vertical transport of gaseous species occurs by the eddy diffusion coefficient derived from the work of *Massie and Hunten* [1981].

The simulation period is set to 10 years to ensure the gas mixtures have enough time to diffuse into the upper atmosphere to participate in the reactions, and each species can achieve the steady state from production and removal processes.

3 CS_2 Reaction Pathways

CS_2 has strong regional and near-surface distribution characteristics [*Bandy et al.*, 1981], indicating active sinks in the CS_2 reaction network. The main reaction channels are illustrated in **Figure 2**, where, despite the dry deposition, the main sink of CS_2 comes from the competition between the OH-oxidation and photo-oxidation pathways. The full CS_2 reaction network is listed in **Table A1** and **Table A2**. More details of these two pathways are discussed below.

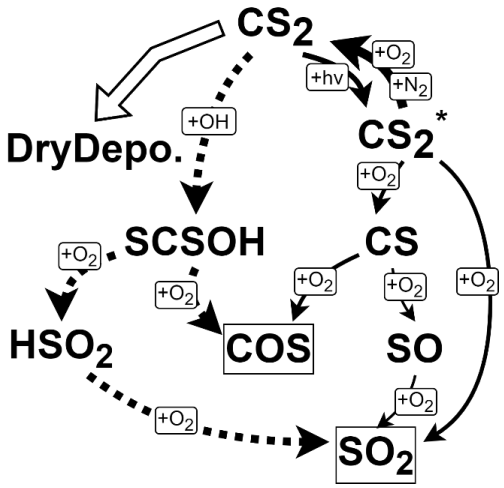

Figure 2. The main reaction pathways of CS_2 in the atmosphere. Each sulfide reactant represents a node in the reaction network. Despite the dry deposition occurring at the surface, the main competition is between the OH oxidation pathway and the photo-oxidation pathway, and both pathways produce the same end-oxidation products COS and SO_2. The figure does not include branching reactions with sulfur fluxes less than 1%.

3.1 Photo-oxidation pathway

The CS_2 photo-oxidation pathway is the first time added to the 1D chemical transport model. Experiments have been carried out to confirm the existence of CS_2 fluorescence under UV light with a wavelength over 300 nm [*Brus*, 1971; *Lambert and Kimbell*, 1973], implying the transition from ground $X^1\Sigma_g^+$ state to the excited B_2 multiplet component of a $^3A_2$ electronic state ($^1B_2{}^3A_2$ state) [*Sorgo et al.*, 1965], following the rapid quenching reaction with the estimated rate coefficient $k_{R1,R2} \geq 2.5 \times 10^{-11}$ cm^3 $molecule^{-1}$ s^{-1} which occurs mainly through the collision with air molecules (simplified as collision with O_2 and N_2 molecules) [*Brus*, 1971; *Lambert and Kimbell*, 1973; *Wine et al.*, 1981]. The CS_2 photo-excitation (**R28**) and CS_2^* quenching reactions (**R1, R2**) are given below:

$$\text{R28: } CS_2 + \hbar\nu \rightarrow CS_2^*$$

$$\text{R1: } CS_2{}^* + O_2 \rightarrow CS_2 + O_2$$

$$\text{R2: } CS_2{}^* + N_2 \rightarrow CS_2 + N_2$$

The latest high-resolution UV absorption spectrum for CS_2 at 298 K is from the work of *Grosch et al.* [2015] and made available through the MPI-Mainz UV/Vis Spectral Atlas database [*Keller-Rudek et al.*, 2013]. However, cross-section data for many wavelengths longer than 350 nm are still unreliable. Instead, we use the suggested absorption cross-section in the 290-350 nm region from *Burkholder et al.* [2020] for the **R28**.

The end-product analysis experiments reported by *Wood and Heicklen* [1971] revealed the existence of the CS_2 photo-oxidation pathway. They deduced the rate coefficient ratio between O_2 oxidation and quenching reactions that $k_{R3}/k_{R1} \approx 0.05$. The CS_2^* oxidation reaction produces CS and SO_2 according to:

$$\text{R3: } CS_2{}^* + O_2 \rightarrow CS + SO_2$$

The CS radical then undergoes the following four reaction pathways:

$$\text{R10: } CS + O \rightarrow S + CO$$

$$\text{R11: } CS + O_2 \rightarrow COS + O$$

$$\text{R12: } CS + O_2 \rightarrow SO + CO$$

$$\text{R13: } CS + O_3 \rightarrow COS + O_2$$

Considering the atmospheric concentration of O_2 is many orders of magnitude higher than that of $O(^3P)$ and O_3, **R11** and **R12** are the main competing oxidation channels. *Richardson* [1975] presented evidence that the rate coefficient ratio $k_{R11}/k_{R12} > 10$ via a fast-flow study. A more precise determination based on the work of *Black et al.* [1983] suggested the rate coefficient for **R11** as 2.9×10^{-19} cm^3 $molecule^{-1}$ s^{-1}.

The SO radical generated by **R12** is further oxidized to SO_2 through the following three reaction channels:

$$\text{R18: } SO + O_2 \rightarrow SO_2 + O$$

206 $$\text{R19: } SO + O_3 \rightarrow SO_2 + O_2$$

207 $$\text{R20: } SO + OH \rightarrow SO_2 + H$$

208 **R18** dominates due to the relatively high atmospheric content of O_2. The rate coefficient uses
209 *Burkholder et al.* [2020], which takes the average of values computed by *Black et al.* [1982]
210 and *Schurath and Goede* [1984] and presents them in the form of the Arrhenius expression as
211 $1.6 \times 10^{-13} \times \exp(-2280/T)$.

212 3.2 OH-oxidation pathway

213 The OH oxidation pathway produces the same oxidation end-products as the photo-oxidation
214 pathway. The two initial reactions are given below:

215 $$\text{R4: } CS_2 + OH \rightarrow COS + SH$$

216 $$\text{R5: } CS_2 + OH \rightarrow SCSOH$$

217 Experimental evidence shows that **R4** proceeds very slowly as a direct bimolecular process at
218 298 K and 1 atm [*Iyer and Rowland*, 1980; *Wine et al.*, 1980]. An upper limit of 2×10^{-15}
219 $cm^3\ molecule^{-1}\ s^{-1}$ for k_{R5} (298K) was suggested by *Burkholder et al.* [2020].

220 **R5** dominates the initial reaction in the OH-oxidation pathway, and it has been observed that
221 the existence of O_2 has an accelerating effect [*Barnes et al.*, 1983; *Hynes et al.*, 1988; *Jones et*
222 *al.*, 1982]. Moreover, several experiments demonstrated the **R5** reaction process that the adduct
223 formation followed by the adduct decomposition in competition with the long-lived adduct
224 oxidation reaction R6 [*Hynes et al.*, 1988; *Murrells et al.*, 1990]:

225 $$\text{R6: } SCSOH + O_2 \rightarrow COS + HSO_2$$

226 The molecule structure configuration of the adduct SCSOH follows theoretical studies which
227 provided evidence that the formation of the S-adduct SCS-OH followed by the addition of O_2
228 to the carbon atom in the initial step. A subsequent step appears to be the transfer of an $O(^3P)$
229 atom to the sulfur-bearing hydroxyl group, leading directly to the formation of COS and HSO_2
230 as shown in **R6** [*McKee and Wine*, 2001; *Luning Zhang and Qin*, 2000]. A more recent density
231 functional theory calculation of the energy and intermediate molecule structures gave
232 theoretical support for the priority production of the S-adduct in the atmospheric condition
233 [*Zeng et al.*, 2017].

234 The negative temperature-dependent rate coefficient was determined in the experiment by
235 *Hynes et al.* [1988] experiment and the effective k_{R5} was suggested as $(1.25 \times$
236 $10^{-16} \exp(4550/T))/(T + 1.81 \times 10^{-3} \exp(3400/T))$ $cm^3\ molecule^{-1}\ s^{-1}$. Besides, the
237 subsequent adduct oxidation $k_{R6} = 2.8 \times 10^{-14}\ cm^3\ molecule^{-1}\ s^{-1}$ takes the suggestion
238 from *Burkholder et al.* [2020]. The molecule rearrangement step for the adduct is simplified
239 and not included as an independent reaction in this study considering that the effective rate
240 coefficient is used.

241 The HSO_2 generated in **R6** will be oxidized rapidly through **R26** as shown below:

242 $$\text{R26: } HSO_2 + O_2 \rightarrow SO_2 + HO_2$$

That *Lovejoy et al.* [1990] found the formation of SO_2 and HO_2 are equal and near unity in the experiment. His later work showed that the ^{18}O atom in the ^{18}OH reactant is transferred predominantly $(90 \pm 20)\%$ to the SO_2 product, indicating the S-O bonded SCS-OH adduct formation and the preservation of the S-O bind in the steps leading to SO_2 formation as described in **R26** [*Lovejoy et al.*, 1994]. The rate coefficient data takes the suggestion from *Burkholder et al.* [2020] as $k_{R26} = 3.0 \times 10^{-13}$ cm^3 molecule^{-1} s^{-1}.

4 Results & Discussions

4.1 Sulfur Flux Analysis of CS_2 Reaction Network

In order to understand the rate of CS_2 conversion among its different oxidation channels, we performed a sulfur flux analysis based on the model-derived reaction rates. The analysis shows the mechanism of the detailed CS_2 oxidation pathways. For the flux flow at a particular sulfide reactant node in the reaction network as shown in **Figure 2**, we used the concept of local consumption to illustrate the percentage of a target element flux from the reactant to each product. The equation is shown as:

$$L_{r_i,S} = \frac{r_i}{\sum_{j=1}^{m} r_j} \times 100\%$$

Where $L_{r_i,S}$ is the percentage consumption of species S in reaction r_i; and m is the number of reactions consuming species S.

The local consumption condition at the node of the initial reactant CS_2 is shown in **Figure 3**, that at the surface, 88.8% of CS_2 molecules participate in the photo-excitation reaction **R28** to produce the excited state CS_2^*, only 5.4% of CS_2 molecules participate in the OH-addition reaction **R5** to form the relatively long-lived S-adduct SCSOH, and 5.8% of CS_2 are removed by dry deposition. With increasing altitude, the ratio of CS_2 participating in the photo-excitation reaction reaches its maximum of 95.5% at 3 km, gradually decreasing to 88.7% at 10 km. The result shows that the photo-excitation reaction in the photo-oxidation pathway dominates in the initial reactions of the CS_2 reaction network.

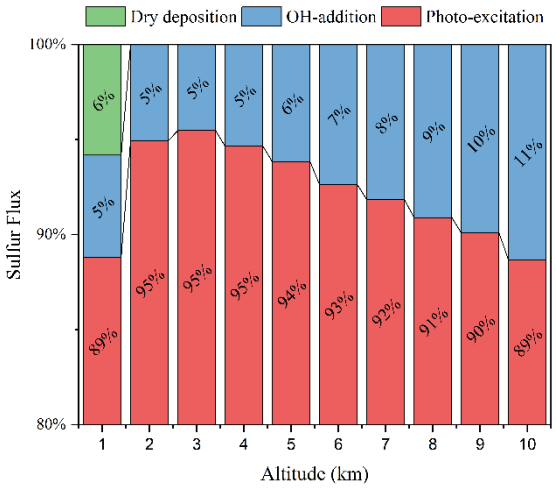

Figure 3. Local consumption situation of CS_2 initial reactions at each height in 1-10 km.

However, most excited state CS_2^* molecules formed by photo-excitation reactions are quenched back to the ground state collision with N_2 and O_2 molecules [*Wine et al.*, 1981]. **Figure 4** shows the local consumption situation at the node of CS_2^* between 1 and 10 km, about 99% of excited CS_2^* molecules are quenched to the ground state through **R1** and **R2**, and only 1% of CS_2^* molecules are further oxidized through reaction **R3** to form CS radical and SO_2. The highly reactive intermediate CS_2^* is in a pseudo-steady state of the CS_2-CS_2^* equilibrium where CS_2^* is consumed virtually as rapidly as they are formed and consequently exist at very low concentrations.

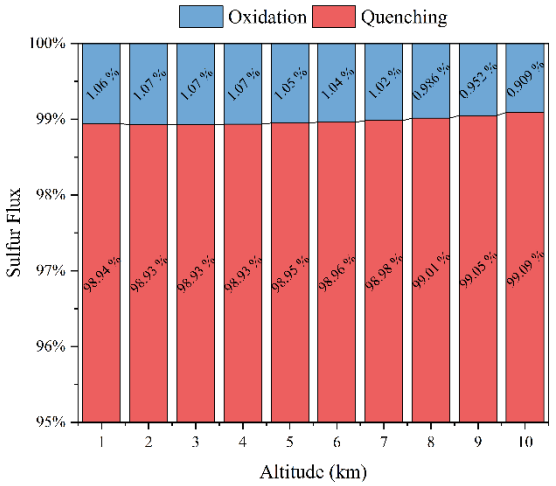

Figure 4. Local consumption situation at the node of CS_2^* at each height in 1-10 km.

The CS radical formed from the CS_2^* oxidation reaction **R3** is further oxidized through several reaction channels, where **R11** and **R12** play a major role, consuming about 90% and 9% of the sulfur flux, respectively. However, the result is based on the reaction coefficients inferred from previous studies using the product ratio method [*Black et al.*, 1983; *Richardson*, 1975] and

more accurate and targeted experiments are needed. In conclusion, the photo-oxidation pathway gives a product ratio COS:SO_2≈9:11 as shown in **Figure 5**. Meanwhile, in the OH-oxidation pathway, **R4** is too slow to occur in the atmosphere and **R5** dominates as the initial reaction of the OH-oxidation pathway that forms the S-adduct SCSOH. The following oxidation reactions **R6** and **R26** are fast and produce COS and SO_2 in the ratio of 1:1.

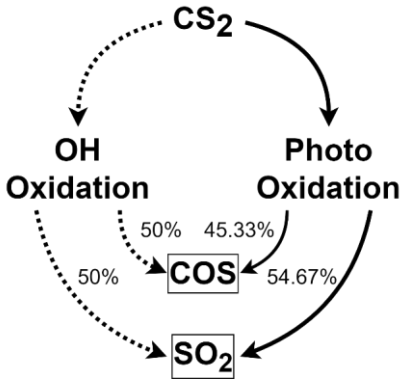

Figure 5. Sulfur flux ratio in each oxidation pathway.

A comparison of reaction rates between the S-adduct SCSOH oxidation reaction **R6** and excited state CS_2^* oxidation reaction **R3** at different altitudes was conducted to determine the proportion of sulfur flux through the two oxidation pathways. This is in consideration of the fact that most of the CS_2^* returns to the ground state and that the oxidation reactions of both intermediates are irreversible. This means that once the sulfur flux passes through the intermediate reactions **R3** and **R6** and will eventually be converted to the end-oxidation products COS and SO_2. The red line in **Figure 6** illustrates the proportion of sulfur flux that passes through the photo-oxidation pathway under the global average solar radiation condition. The figure also shows that about 15% of the sulfur flux is involved in the photo-oxidation pathway at the surface. This ratio reaches its peak at 3 km, which is about 18%, and gradually decreases to 7% at 10 km. For a vertical distribution, a concentration-weighted average 15.8% of the sulfur flux passes through the photo-oxidation pathway.

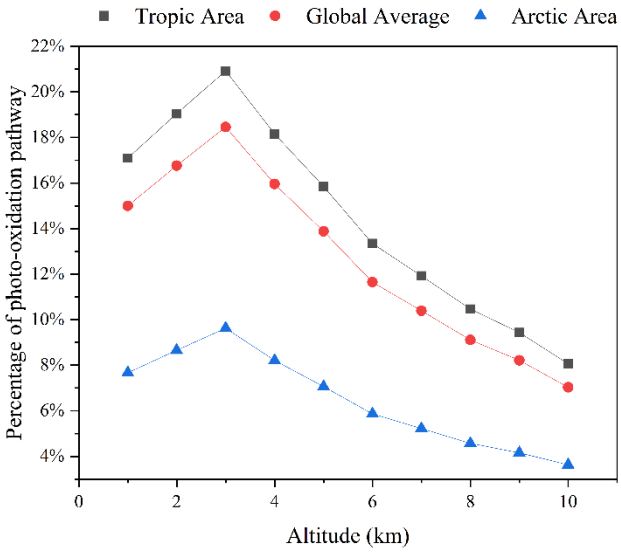

Figure 6. The percentage of sulfur flux passes through the photo-oxidation pathway in the two main CS_2 sink pathways at each altitude in 1-10 km.

The above results are all based on solar irradiance using the daytime-weighted method [*Cronin*, 2014] that represents the global average irradiance level of about 342 W/m^2. The annual mean solar irradiance received at different latitudes on Earth varies approximately from 160 W/m^2 in the arctic area to 400 W/m^2 in the tropic area [*Liou*, 1980]. To investigate the ratio of CS_2 oxidized through the photo-oxidation pathway under different solar irradiance conditions, we also performed a sulfur flux analysis for each radiation condition and the results are shown as the black and blue line in **Figure 6**. As expected, more sulfur fluxes enter the photo-oxidation pathway under stronger solar irradiance condition. At low latitudes in the tropic region where sunlight is strongest on average, about 17% of the surface oxidized CS_2 passes through the photo-oxidation pathway to produce COS and SO_2, and this proportion reaches about 21% at 3 km. Even in the polar regions at high latitudes, where the average annual solar irradiance is less than half the global average, the sulfur flux in the photo-oxidation pathway is nearly 8% at the surface, again peaking at about 10% at 3 km altitude. All these results show that the photo-oxidation pathway shares an important proportion in the atmospheric removal of CS_2. Taking the concentration-weighted method as above, at low latitudes with the highest sunlight radiation (400 W/m^2) and high latitudes with the lowest sunlight radiation (160 W/m^2), 18% and 8.1% of the sulfur flux passes through the photo-oxidation pathway in the two main sink pathways of CS_2, respectively.

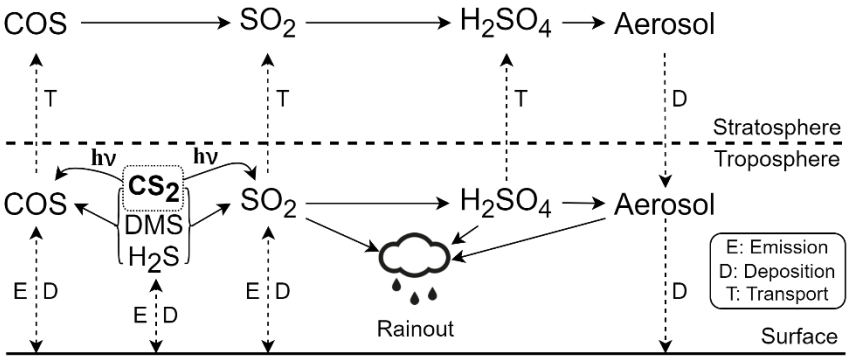

Figure 7. The schematic diagram of the reproduced atmospheric sulfur cycle in this study with the addition of the CS_2 photo-oxidation pathway.

4.2 Effect of photo-oxidation pathway on atmospheric COS

The introduction of the photo-oxidation pathway to the CS_2 reaction network changes the original product balance according to the sulfur flux analysis above. To investigate the effect of the CS_2 photo-oxidation pathway in the atmospheric sulfur cycle, we add the CS_2 reaction network to the sulfur cycle with the schematic diagram as illustrated in **Figure 7**. The scheme shows the main channels for generating COS and SO_2, from oxidation of atmospheric reduced sulfur species as well as the further production of sulfate aerosols and its removal from the atmosphere by deposition processes. The emission and deposition data are listed in **Table 1**. The process of aerosol formation, including complex physical condensation and chemical reactions, is simplified in this study. The formation of sulfuric acid aerosol is based on the scheme proposed by *Hamill et al.* [1977]. This aerosol formation scheme proposes that aggregated nuclei are formed under the condition where partial pressure versus vapor pressure is larger than 1. The sulfuric acid aerosol particle size was assumed to be 0.3 μm, and the gravitational deposition velocity was taken from *Kasten* [1968]. The additional reactions added to the CS_2 reaction network are listed in **Table A3** and **Table A4**.

The model reproduced the vertical distribution of CS_2, COS, and SO_2 in the atmosphere as shown in **Figure 8**. The CS_2 concentration at surface is calculated as 2.69 pptv, which compares favorably with the estimated range in the free troposphere [*Bandy et al.*, 1981] and reported field measurement [*Khalil and Rasmussen*, 1984] and decreases rapidly with increasing altitudes and is below 0.01 pptv over 10 km. The modeled COS concentration at surface is 521.62 pptv which compares favorably with tropospheric field measurements [*Carroll*, 1985; *Maroulis et al.*, 1977; *Torres et al.*, 1980], and when it rises to the stratosphere, the photolysis reaction rapidly depletes COS resulting in a sharp decrease in concentration. The high uncertainty of SO_2 dry deposition rates could cause the deviation of SO_2 concentration [*Garland*, 1977; *Seinfeld and Pandis*, 2006], and modeled SO_2 is 288.4 pptv at surface which is within the estimated range of the background troposphere [*Jacobson*, 2005]. With increasing altitude, the SO_2 concentration decreases faster than the measured values [*Höpfner et al.*, 2015], and when it comes to the upper atmosphere over 35 km, the simulated SO_2 concentration is

lower than the measured data [*Rinsland et al.*, 1995]. The most likely source of errors is likely related to the uncertainties associated with the photodissociation process of molecular H_2SO_4 prior formation of SSA. Considering that the SSA generation scheme is simplified and that SO_2 is not the main objective of this study, the difference in SO_2 concentration between the model simulation and field measurements is within one order of magnitude. We thus assume the overall result is reasonable. The other sulfur compounds DMS, H_2S, H_2SO_4, and aerosol are all compared favorably with field measurements [*Jacobson*, 2005; *Maroulis and Bandy*, 1977; *Turco et al.*, 1979].

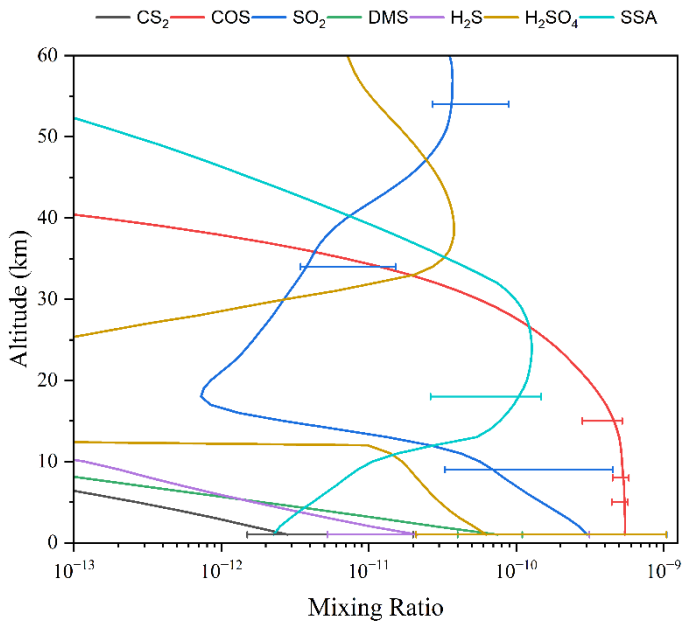

Figure 8. The vertical distribution of sulfur compounds in the reproduced sulfur cycle.

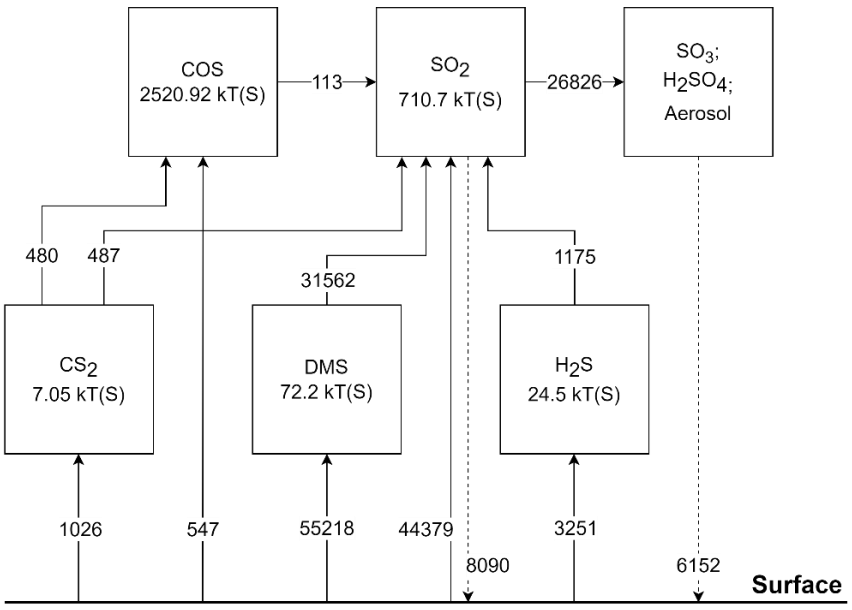

Figure 9. Schematic diagram of the sulfate budget in the model. Boxes show the sulfur quantity of each sulfate in the unit of kilotons of sulfur. Solid line arrows show net sulfur fluxes of sulfate emissions from the surface and chemical exchange rates in the unit of kilotons of sulfur per year. Dashed lines with arrows show the washout sulfur fluxes with the same unit used in solid line arrows.

A schematic diagram of the sulfur budget from this model study is shown in **Figure 9**, where each sulfur gas burden is shown in the box in kiloton of sulfur units. The solid line arrows represent the net sulfur fluxes of sulfur emissions from the surface and chemical exchange rates in kilotons of sulfur per year units, and the dashed line arrows represent the washout sulfur fluxes in kilotons of sulfur per year units. The complex oxidation processes of DMS in the atmosphere were simplified under the scheme presented by *Weisenstein et al.* [1997], and only the conversion of DMS to SO_2 was used since the other minor product MSA is not relevant to this study. Sulfides associated with aerosol formation such as SO_3, H_2SO_4, and aerosols are considered a single chemical species, therefore the sulfur quantity for minor sulfide species might have discrepancies with the real atmosphere. The aerosols sections are added mainly for atmospheric removal of other sulfides to achieve the model's mass balance and sulfide equilibrium.

Surface emission brings 1026 kilotons of sulfur per year to the global CS_2 burden, and CS_2 contributes 480 kilotons of sulfur per year to the COS burden and 487 kilotons of sulfur per year to the SO_2 burden, leading to 7.05 kilotons of sulfur in CS_2 burden after deposition processes. The COS/CS_2 product balance change from adding the new CS_2 photo-oxidation pathway is about 1.5%. The CS_2 lifetime in the troposphere is about 2 to 3 days from model estimation and consistent with values reported by *Khan et al.* [2017]. About 47% of atmospheric COS burden comes from the chemical transformation of CS_2. Combined with the sulfur flux analysis results above, about 5% of the COS at surface comes from the CS_2 photo-oxidation pathway under the global average solar radiation condition. Meanwhile, the impact of CS_2 on atmospheric SO_2 is relatively small, mainly because SO_2 has large emissions from the surface and a significant amount of chemical transformations from DMS and H_2S, compared to the relatively minor sulfur flux from CS_2 chemical transformations. In summary, the photo-oxidation pathway accounts for an important share of the atmospheric CS_2 sink, but its introduction brings relatively small changes to the global COS and SO_2 concentrations.

5 Conclusion

In this study, we have constructed a 1D model of the CS_2 reaction network and extended it to a sulfur cycle. The daytime-weighted zenith angle and solar constant are applied to counteract the spatial-temporal variation and simulate the global average solar radiation. Modeled sulfur-bearing species concentrations reproduced field measurements or other model estimations. From the sulfur flux analysis, we found that the photo-oxidation and OH-oxidation pathways contain near-magnitude sulfur fluxes in the CS_2 reaction network and that 15.8% of sulfur flux

404 passes through the photo-oxidation pathway under global average solar irradiance condition.
405 Depending on the local solar radiation intensity, this proportion ranges from 8.1% to 18%. The
406 sulfur budget of the sulfur cycle in this study is determined and it is concluded that the addition
407 of the CS_2 photo-oxidation pathway has a relatively minor change (1.5%) on the product ratio
408 between COS and SO_2. Nevertheless, it is still recommended to include the photo-oxidation
409 pathway of CS_2 in future model studies, considering the important proportion of the photo-
410 oxidation pathway in the CS_2 sink.

411

412 **Appendix**

413 **Table A1: Non-photochemistry reaction in the CS_2 reaction network.**

No.	Reaction	Rate Constant	References
1	$CS_2^*+O_2 \rightarrow CS_2$	2.5×10^{-11}	*Brus* [1971]; *Lambert and Kimbell* [1973]
2	$CS_2^*+N_2 \rightarrow CS_2$	2.5×10^{-11}	*Brus* [1971]; *Lambert and Kimbell* [1973]
3	$CS_2^*+O_2 \rightarrow CS+SO_2$	1.25×10^{-12}	*Wood and Heicklen* [1971]
4	$CS_2+OH \rightarrow COS+SH$	2×10^{-15}	*Burkholder et al.* [2020]
5	$CS_2+OH \rightarrow SCSOH$	$(1.25\times10^{-16}\times\exp(4550/T))/(T+1.81\times10^{-3}\exp(3400/T))$	*Burkholder et al.* [2020]
6	$SCSOH+O_2 \rightarrow COS+HSO_2$	2.8×10^{-14}	*Burkholder et al.* [2020]
7	$CS_2+O \rightarrow CS+SO$	$3.2\times10^{-11}\times\exp(-650/T)$	*Burkholder et al.* [2020]
8	$CS_2+O \rightarrow COS+S$	$2.72\times10^{-12}\times\exp(-650/T)$	*Burkholder et al.* [2020]
9	$CS_2+O \rightarrow S_2+CO$	$9.6\times10^{-13}\times\exp(-650/T)$	*Burkholder et al.* [2020]
10	$CS+O \rightarrow S+CO$	$2.7\times10^{-10}\times\exp(-760/T)$	*Burkholder et al.* [2020]
11	$CS+O_2 \rightarrow COS+O$	2.9×10^{-19}	*Burkholder et al.* [2020]
12	$CS+O_2 \rightarrow SO+CO$	2.9×10^{-20}	*Burkholder et al.* [2020]
13	$CS+O_3 \rightarrow COS+O_2$	3.0×10^{-16}	*Burkholder et al.* [2020]
14	$S+O_2 \rightarrow SO+O$	$1.6\times10^{-12}\times\exp(100/T)$	*Burkholder et al.* [2020]
15	$S+O_3 \rightarrow SO+O_2$	1.2×10^{-11}	*Burkholder et al.* [2020]
16	$S+OH \rightarrow SO+H$	6.6×10^{-11}	*Burkholder et al.* [2020]
17	$S_2+O \rightarrow S+SO$	1.6×10^{-13}	*Hills et al.* [1987]; *Singleton and Cvetanović* [1988]
18	$SO+O_2 \rightarrow SO_2+O$	$1.6\times10^{-13}\times\exp(-2280/T)$	*Burkholder et al.* [2020]
19	$SO+O_3 \rightarrow SO_2+O_2$	$3.4\times10^{-12}\times\exp(-1100/T)$	*Burkholder et al.* [2020]
20	$SO+OH \rightarrow SO_2+H$	$2.6\times10^{-11}\times\exp(330/T)$	*Burkholder et al.* [2020]
21	$SH+O \rightarrow SO+H$	1.6×10^{-10}	*Burkholder et al.* [2020]
22	$SH+O_2 \rightarrow SO+OH$	4.0×10^{-19}	*Burkholder et al.* [2020]
23	$SH+O_3 \rightarrow HSO+O_2$	$9.0\times10^{-12}\times\exp(-280/T)$	*Burkholder et al.* [2020]
24	$HSO+O_2 \rightarrow SO_2+OH$	2.0×10^{-17}	*Burkholder et al.* [2020]
25	$HSO+O_3 \rightarrow SO_2+SH$	1.0×10^{-13}	*Burkholder et al.* [2020]
26	$HSO_2+O_2 \rightarrow SO_2+HO_2$	3.0×10^{-13}	*Burkholder et al.* [2020]

414

415

416 **Table A2: Photochemistry reactions in the CS_2 reaction network.**

417

No.	Reaction	References
27	$CS_2+hv \rightarrow CS+S$	180-194 nm: *Chen and Robert Wu* [1995] 194-205 nm: *Sunanda et al.* [2015] 205-275 nm: *Grosch et al.* [2015]
28	$CS_2+hv \rightarrow CS_2^*$	275-370 nm: *Burkholder et al.* [2020] 370-400 nm: No data
29	$SO+hv \rightarrow S+O$	180-260 nm: *Danielache et al.* [2014] 260-400 nm: No data

418 **Table A3: Additional non-photochemical reactions that constitute the complete sulfur**
419 **cycle.**

420

No.	Reaction	Rate Constant	References
30	COS+OH→CO2+SH	1.1×10-13×exp(-1200/T)	*Burkholder et al.* [2020]
31	COS+O→CO+SO	$2.1\times10^{-11}\times\exp(-2200/T)$	*Burkholder et al.* [2020]
32	H_2S+OH→H_2O+SH	$6.1\times10^{-12}\times\exp(-75/T)$	*Burkholder et al.* [2020]
33	H_2S+O→OH+SH	$9.22\times10^{-12}\times\exp(-1803/T)$	*Burkholder et al.* [2020]
34	H_2S+H→H_2+SH	8×10^{-13}	*Burkholder et al.* [2020]
35	H_2S+HO_2→H_2O+HSO	3×10^{-15}	*Burkholder et al.* [2020]
36	SO_2+HO_2→OH+SO_3	1×10^{-18}	*Burkholder et al.* [2020]
37	SO_2+O_3→O_2+SO_3	$3\times10^{-12}\times\exp(-7000/T)$	*Burkholder et al.* [2020]
38	HSO_3+O_2→HO_2+SO_3	$1.3\times10^{-12}\times\exp(-330/T)$	*Burkholder et al.* [2020]
39	SO_2+O→SO_3	$1.80\times10^{-33}\times(T/300)^{2}$	*Burkholder et al.* [2020]
40	SO_2+OH→HSO_3	$3.30\times10^{-31}\times(T/300)^{-4.3}$	*Burkholder et al.* [2020]
41	SO_3+H_2O→H_2SO_4	1.2×10^{-15}	*Burkholder et al.* [2020]
42	H_2SO_4→SO_2+2OH	1.2×10^{-15}	*Burkholder et al.* [2020]
43	CH_3SCH_3+O→SO_2	$1\times10^{-11}\times\exp(410/T)$	*Weisenstein et al.* [1997]
44	CH_3SCH_3+OH→SO_2	$1.2\times10^{-11}\times\exp(-260/T)$	*Weisenstein et al.* [1997]
45	CH_3SCH_3+OH→ SO_2+CH_4O_3S	$3.04\times10^{-12}\times\exp(350/T)$	*Weisenstein et al.* [1997]
46	SO_2→SO_4		

421 **Table A4: Additional photochemical reactions that constitute the complete sulfur cycle.**

422

No.	Reaction	References
47	$COS+hv \rightarrow CO+S$	180-185 nm: No data 185-195 nm: *Limão-Vieira et al.* [2015] 195-260 nm: *Hattori et al.* [2011] 260-300 nm: *Limão-Vieira et al.* [2015] 300-400 nm: No data
48	$SO_2+hv \rightarrow SO+O$	180-189.5 nm : *Danielache et al.* [2008] 189.5-225 nm: *Endo et al.* [2015] 225-239 nm: *Wu et al.* [2000] 239-400 nm: *Bogumil et al.* [2003]
49	$O_3+hv \rightarrow O_2+O$	180-230 nm: *Burkholder et al.* [2020] 230-400 nm: *Malicet et al.* [1995]
50	$O_2+hv \rightarrow 2O$	180-181 nm: *Kockarts* [1976] 181-235 nm: *Ogawa* [1971] 235-400 nm: *Bogumil et al.* [2003]
51	$SO_3+hv \rightarrow SO_2+O$	180-330 nm: *Burkholder et al.* [2020] 330-400 nm: No data
52	$H_2S+hv \rightarrow SH+H$	180-260 nm: *Wu and Chen* [1998] 260-370 nm: *Grosch et al.* [2015] 370-400 nm: No data

References

Avila, P. J., T. Grassi, S. Bovino, A. Chiavassa, B. Ercolano, S. O. Danielache, and E. Simoncini (2021), Presence of water on exomoons orbiting free-floating planets: a case study, *Int J Astrobiol*, *20*(4), 300-311, doi:10.1017/S1473550421000173.

Bandy, A. R., P. J. Maroulis, L. Shalaby, and L. A. Wilner (1981), Evidence for a short tropospheric residence time for carbon-disulfide, *Geophys Res Lett*, *8*(11), 1180-1183, doi:10.1029/GL008i011p01180.

Barnes, I., K. Becker, E. Fink, A. Reimer, F. Zabel, and H. Niki (1983), Rate constant and products of the reaction CS_2 + OH in the presence of O_2, *International journal of chemical kinetics*, *15*(7), 631-645, doi:10.1002/kin.550150705.

Bates, D. (1984), Rayleigh scattering by air, *Planetary and Space Science*, *32*(6), 785-790.

Belviso, S., M. Schmidt, C. Yver, M. Ramonet, V. Gros, and T. Launois (2013), Strong similarities between night-time deposition velocities of carbonyl sulphide and molecular hydrogen inferred from semi-continuous atmospheric observations in Gif-sur-Yvette, Paris region, *Tellus B: Chemical and Physical Meteorology*, *65*(1), 20719, doi:10.3402/tellusb.v65i0.20719.

Black, G., L. Jusinski, and T. Slanger (1983), Rate coefficients for CS reactions with O_2, O_3 and NO_2 at 298 K, *Chemical physics letters*, *102*(1), 64-68, doi:10.1016/0009-2614(83)80659-9.

Black, G., R. Sharpless, and T. Slanger (1982), Rate coefficients for SO reactions with O_2 and O_3 over the temperature range 230 to 420 K, *Chemical Physics Letters*, *93*(6), 598-602, doi:10.1016/0009-2614(82)83737-8.

Bogumil, K., J. Orphal, T. Homann, S. Voigt, P. Spietz, O. Fleischmann, A. Vogel, M. Hartmann, H. Kromminga, and H. Bovensmann (2003), Measurements of molecular absorption spectra with the SCIAMACHY pre-flight model: instrument characterization and reference data for atmospheric remote-sensing in the 230–2380 nm region, *Journal of Photochemistry and Photobiology A: Chemistry*, *157*(2-3), 167-184, doi:10.1016/S1010-6030(03)00062-5.

Brühl, C., J. Lelieveld, P. J. Crutzen, and H. Tost (2011), The role of carbonyl sulphide as a source of stratospheric sulphate aerosol and its impact on climate, *Atmospheric Chemistry and Physics*, *12*, 1239-1253, doi:10.5194/ACP-12-1239-2012.

Brus, L. (1971), Two exponential decay of 3371 Å laser excited CS_2 fluorescence, *Chemical Physics Letters*, *12*(1), 116-119, doi:10.1016/0009-2614(71)80629-2.

Burkholder, J., et al. (2020), Chemical kinetics and photochemical data for use in atmospheric studies; evaluation number 19*Rep.*, Pasadena, CA: Jet Propulsion Laboratory, National Aeronautics and Space ….

Carroll, M. A. (1985), Measurements of OCS and CS_2 in the free troposphere, *Journal of Geophysical Research: Atmospheres*, *90*(D6), 10483-10486, doi:10.1029/JD090iD06p10483.

Chen, F., and C. Robert Wu (1995), High, room and low temperature photoabsorption cross sections of CS2 in the 1800–2300 Å region, *Geophys Res Lett*, *22*(16), 2131-2134, doi:10.1029/95GL01898.

Chin, M., and D. Davis (1993), Global sources and sinks of OCS and CS_2 and their distributions, *Global Biogeochemical Cycles*, *7*(2), 321-337, doi:10.1029/93gb00568.

Colman, J. J., and W. C. Trogler (1997), The long‐wavelength photochemistry of carbon

disulfide, *Journal of Geophysical Research: Atmospheres*, *102*(D15), 19029-19041, doi:10.1029/97JD00401.
Cope, D., and D. Spedding (1982), Hydrogen sulphide uptake by vegetation, *Atmospheric Environment (1967)*, *16*(2), 349-353, doi:10.1016/0004-6981(82)90452-8.
Cronin, T. W. (2014), On the choice of average solar zenith angle, *Journal of the Atmospheric Sciences*, *71*(8), 2994-3003, doi:10.1175/JAS-D-13-0392.1.
Crutzen, P. J. (1976), The possible importance of CSO for the sulfate layer of the stratosphere, *Geophys Res Lett*, *3*(2), 73-76, doi:10.1029/GL003i002p00073.
Danielache, S. O., C. Eskebjerg, M. S. Johnson, Y. Ueno, and N. Yoshida (2008), High-precision spectroscopy of 32S, 33S, and 34S sulfur dioxide: Ultraviolet absorption cross sections and isotope effects, *Journal of Geophysical Research: Atmospheres*, *113*(D17), doi:10.1029/2007JD009695.
Danielache, S. O., G. Iwama, M. Shinkai, M. Oinuma, E. Simoncini, and T. Grassi (2023), Introducing Atmospheric Photochemical Isotopic Processes to the PATMO atmospheric code, *GEOCHEMICAL JOURNAL*, *advpub*, doi:10.2343/geochemj.GJ23004.
Danielache, S. O., S. Tomoya, A. Kondorsky, I. Tokue, and S. Nanbu (2014), Nonadiabatic calculations of ultraviolet absorption cross section of sulfur monoxide: isotopic effects on the photodissociation reaction, *The Journal of chemical physics*, *140*(4), 044319, doi:10.1063/1.4862429.
Endo, Y., S. O. Danielache, Y. Ueno, S. Hattori, M. S. Johnson, N. Yoshida, and H. G. Kjaergaard (2015), Photoabsorption cross-section measurements of 32S, 33S, 34S, and 36S sulfur dioxide from 190 to 220 nm, *Journal of Geophysical Research: Atmospheres*, *120*(6), 2546-2557, doi:10.1002/2014JD021671.
Fu, Q., and K. N. Liou (1993), Parameterization of the radiative properties of cirrus clouds, *Journal of Atmospheric Sciences*, *50*(13), 2008-2025, doi:10.1175/1520-0469(1993)050<2008:potrpo>2.0.co;2.
Garland, J. (1977), The dry deposition of sulphur dioxide to land and water surfaces, *Proceedings of the Royal Society of London. A. Mathematical and Physical Sciences*, *354*(1678), 245-268, doi:10.1098/rspa.1977.0066.
Giorgi, F., and W. Chameides (1985), The rainout parameterization in a photochemical model, *Journal of Geophysical Research: Atmospheres*, *90*(D5), 7872-7880, doi:10.1029/JD090iD05p07872.
Grosch, H., A. Fateev, and S. Clausen (2015), UV absorption cross-sections of selected sulfur-containing compounds at temperatures up to 500 °C, *Journal of Quantitative Spectroscopy and Radiative Transfer*, *154*, 28-34, doi:10.1016/j.jqsrt.2014.11.020.
Hajer, M. A. (2002), Discourse coalitions and the institutionalization of practice: the case of acid rain in Great Britain, in *Argument turn policy anal plan*, edited, pp. 51-84, Routledge.
Hamill, P., O. Toon, and C. Kiang (1977), Microphysical processes affecting stratospheric aerosol particles, *Journal of Atmospheric Sciences*, *34*(7), 1104-1119, doi:10.1175/1520-0469(1977)034<1104:mpasap>2.0.co;2.
Hattori, S., S. Danielache, M. Johnson, J. Schmidt, H. Kjaergaard, S. Toyoda, Y. Ueno, and N. Yoshida (2011), Ultraviolet absorption cross sections of carbonyl sulfide isotopologues $OC^{32}S$,

$OC^{33}S$, $OC^{34}S$ and $O^{13}CS$: isotopic fractionation in photolysis and atmospheric implications, *Atmospheric Chemistry and Physics*, *11*(19), 10293-10303, doi:10.5194/acp-11-10293-2011.

He, Q., Z. Fang, O. Shoshanim, S. S. Brown, and Y. Rudich (2021), Scattering and absorption cross sections of atmospheric gases in the ultraviolet–visible wavelength range (307–725 nm), *Atmospheric Chemistry and Physics*, *21*(19), 14927-14940.

Hills, A. J., R. J. Cicerone, J. G. Calvert, and J. W. Birks (1987), Kinetics of the reactions of diatomic sulfur with atomic oxygen, molecular oxygen, ozone, nitrous oxide, nitric oxide, and nitrogen dioxide, *Journal of Physical Chemistry*, *91*(5), 1199-1204, doi:10.1021/j100289a033.

Höpfner, M., C. Boone, B. Funke, N. Glatthor, U. Grabowski, A. Günther, S. Kellmann, M. Kiefer, A. Linden, and S. Lossow (2015), Sulfur dioxide (SO_2) from MIPAS in the upper troposphere and lower stratosphere 2002–2012, *Atmospheric Chemistry and Physics*, *15*(12), 7017-7037, doi:10.5194/acp-15-7017-2015.

Hu, R., S. Seager, and W. Bains (2012), Photochemistry in terrestrial exoplanet atmospheres. I. Photochemistry model and benchmark cases, *The Astrophysical Journal*, *761*(2), 166, doi:10.1088/0004-637X/761/2/166.

Hynes, A. J., P. Wine, and J. Nicovich (1988), Kinetics and mechanism of the reaction of hydroxyl with carbon disulfide under atmospheric conditions, *The Journal of Physical Chemistry*, *92*(13), 3846-3852, doi:10.1021/j100324a034.

Iyer, R. S., and F. Rowland (1980), A significant upper limit for the rate of formation, of OCS from the reaction of OH with CS_2, *Geophys Res Lett*, *7*(10), 797-800, doi:10.1029/GL007i010p00797.

Jacobson, M. Z. (2005), *Fundamentals of Atmospheric Modeling*, 2 ed., Cambridge University Press, Cambridge, doi:10.1017/CBO9781139165389.

Jones, B., J. Burrows, R. Cox, and S. Penkett (1982), OCS formation in the reaction of OH with CS_2, *Chemical Physics Letters*, *88*(4), 372-376, doi:10.1016/0009-2614(82)83028-5.

Judeikis, H. S., and A. G. Wren (1977), Deposition of H_2S and dimethyl sulfide on selected soil materials, *Atmospheric Environment (1967)*, *11*(12), 1221-1224, doi:10.1016/0004-6981(77)90099-3.

Kasten, F. (1968), Falling speed of aerosol particles, *Journal of Applied Meteorology (1962-1982)*, *7*(5), 944-947, doi:10.1175/1520-0450(1968)007<0944:fsoap>2.0.co;2.

Keller-Rudek, H., G. Moortgat, R. Sander, and R. Sörensen (2013), The MPI-Mainz UV/VIS spectral atlas of gaseous molecules of atmospheric interest, *Earth System Science Data*, *5*(2), 365-373, doi:10.5194/essd-5-365-2013.

Kerr, J., and V. E. Fioletov (2008), Surface ultraviolet radiation, *Atmosphere-Ocean*, *46*(1), 159-184, doi:10.3137/ao.460108.

Khalil, M., and R. Rasmussen (1984), Global sources, lifetimes and mass balances of carbonyl sulfide (OCS) and carbon disulfide (CS_2) in the earth's atmosphere, *Atmospheric Environment (1967)*, *18*(9), 1805-1813, doi:10.1016/0004-6981(84)90356-1.

Khan, A., B. Razis, S. Gillespie, C. Percival, and D. Shallcross (2017), Global analysis of carbon disulfide (CS_2) using the 3-D chemistry transport model STOCHEM, *AIMS Environmental Science*, *4*(3), 484-501, doi:10.3934/environsci.2017.3.484.

Kjellström, E. (1998), A three-dimensional global model study of carbonyl sulfide in the troposphere and the lower stratosphere, *Journal of Atmospheric Chemistry*, *29*(2), 151-177, doi:10.1016/s0021-8502(97)88129-3.

552 Kockarts, G. (1976), Absorption and photodissociation in the Schumann-Runge bands of
553 molecular oxygen in the terrestrial atmosphere, *Planetary and Space Science*, *24*(6), 589-604,
554 doi:10.1016/0032-0633(76)90137-9.
555 Kremser, S., et al. (2016), Stratospheric aerosol—Observations, processes, and impact on
556 climate, *Reviews of Geophysics*, *54*, 278 - 335, doi:10.1002/2015RG000511.
557 Krueger, A. J., and R. A. Minzner (1976), A mid - latitude ozone model for the 1976 US
558 Standard Atmosphere, *Journal of Geophysical Research*, *81*(24), 4477-4481,
559 doi:10.1029/JC081i024p04477.
560 Lambert, C., and G. Kimbell (1973), The fluorescence of CS_2 vapor, *Canadian Journal of*
561 *Chemistry*, *51*(16), 2601-2608, doi:10.1139/v73-393.
562 Lee, C.-L., and P. Brimblecombe (2016), Anthropogenic contributions to global carbonyl
563 sulfide, carbon disulfide and organosulfides fluxes, *Earth-science reviews*, *160*, 1-18,
564 doi:10.1016/j.earscirev.2016.06.005.
565 Lee, C., R. V. Martin, A. Van Donkelaar, H. Lee, R. R. Dickerson, J. C. Hains, N. Krotkov, A.
566 Richter, K. Vinnikov, and J. J. Schwab (2011), SO_2 emissions and lifetimes: Estimates from
567 inverse modeling using in situ and global, space - based (SCIAMACHY and OMI) observations,
568 *Journal of Geophysical Research: Atmospheres*, *116*(D6), doi:10.1029/2010JD014758.
569 Limão-Vieira, P., F. Ferreira da Silva, D. Almeida, M. Hoshino, H. Tanaka, D. Mogi, T. Tanioka,
570 N. J. Mason, S. V. Hoffmann, and M.-J. Hubin-Franskin (2015), Electronic excitation of
571 carbonyl sulphide (COS) by high-resolution vacuum ultraviolet photoabsorption and electron-
572 impact spectroscopy in the energy region from 4 to 11 eV, *The Journal of Chemical Physics*,
573 *142*(6), 064303, doi:10.1063/1.4907200.
574 Liou, K.-N. (1980), Chapter 2: Solar radiation at the top of the atmosphere, in *International*
575 *Geophysics*, edited by K.-N. Liou, pp. 28-49, Academic Press, doi:10.1016/S0074-
576 6142(08)60677-4.
577 Lovejoy, E. R., T. P. Murrells, A. Ravishankara, and C. J. Howard (1990), Oxidation of carbon
578 disulfide by reaction with hydroxyl. 2. Yields of hydroperoxyl and sulfur dioxide in oxygen,
579 *Journal of Physical Chemistry*, *94*(6), 2386-2393.
580 Lovejoy, E. R., A. Ravishankara, and C. J. Howard (1994), Yield of $^{16}OS^{18}O$ from the ^{18}OH
581 initiated oxidation of CS_2 in $^{16}O_2$, *International journal of chemical kinetics*, *26*(5), 551-560,
582 doi:10.1002/kin.550260508.
583 Malicet, J., D. Daumont, J. Charbonnier, C. Parisse, A. Chakir, and J. Brion (1995), Ozone UV
584 spectroscopy. II. Absorption cross-sections and temperature dependence, *Journal of*
585 *atmospheric chemistry*, *21*(3), 263-273, doi:10.1007/BF00696758.
586 Manabe, S., and R. F. Strickler (1964), Thermal equilibrium of the atmosphere with a
587 convective adjustment, *Journal of the Atmospheric Sciences*, *21*(4), 361-385,
588 doi:10.1175/1520-0469(1964)021%3C0361:TEOTAW%3E2.0.CO;2.
589 Manabe, S., and R. T. Wetherald (1967), Thermal equilibrium of the atmosphere with a given
590 distribution of relative humidity, doi:10.1175/1520-
591 0469(1967)024<0241:TEOTAW>2.0.CO;2.
592 Maroulis, P. J., and A. R. Bandy (1977), Estimate of the contribution of biologically produced
593 dimethyl sulfide to the global sulfur cycle, *Science*, *196*(4290), 647-648,

doi:10.1126/science.196.4290.647.
Maroulis, P. J., A. L. Torres, and A. R. Bandy (1977), Atmospheric concentrations of carbonyl sulfide in the southwestern and eastern United States, *Geophys Res Lett*, *4*(11), 510-512, doi:10.1029/GL004i011p00510.
Massie, S., and D. Hunten (1981), Stratospheric eddy diffusion coefficients from tracer data, *Journal of Geophysical Research: Oceans*, *86*(C10), 9859-9868, doi:10.1029/JC086iC10p09859.
McKee, M. L., and P. Wine (2001), Ab initio study of the atmospheric oxidation of CS_2, *Journal of the American Chemical Society*, *123*(10), 2344-2353, doi:10.1021/ja003421p.
Mills, M. J., et al. (2017), Radiative and Chemical Response to Interactive Stratospheric Sulfate Aerosols in Fully Coupled CESM1(WACCM), *Journal of Geophysical Research: Atmospheres*, *122*, 13,061 - 013,078, doi:10.1002/2017JD027006.
Mopper, K., D. J. Kieber, and A. Stubbins (2015), Marine photochemistry of organic matter: processes and impacts, *Biogeochemistry of marine dissolved organic matter*, 389-450, doi:10.1016/B978-0-12-405940-5.00008-X.
Murrells, T. P., E. R. Lovejoy, and A. Ravishankara (1990), Oxidation of CS_2 by reaction with OH. 1. Equilibrium constant for the reaction OH + CS_2. ⇌ CS_2OH and the kinetics of the CS_2OH + O_2 reaction, *Journal of Physical Chemistry*, *94*(6), 2381-2386, doi:10.1021/j100369a036.
Ogawa, M. (1971), Absorption cross sections of O_2 and CO_2 continua in the Schumann and far-UV regions, *The Journal of Chemical Physics*, *54*(6), 2550-2556, doi:10.1063/1.1675211.
Ramanathan, V. (1976), Radiative transfer within the earth's troposphere and stratosphere: A simplified radiative-convective model, *Journal of Atmospheric Sciences*, *33*(7), 1330-1346, doi:10.1175/1520-0469(1976)033%3C1330:RTWTET%3E2.0.CO;2.
Richardson, R. J. (1975), Carbon monosulfide-oxygen flame reaction chemistry, *The Journal of Physical Chemistry*, *79*(12), 1153-1158.
Rinsland, C., M. Gunson, M. Ko, D. Weisenstein, R. Zander, M. Abrams, A. Goldman, N. Sze, and G. Yue (1995), H_2SO_4 photolysis: A source of sulfur dioxide in the upper stratosphere, *Geophys Res Lett*, *22*(9), 1109-1112, doi:10.1029/95GL00917.
Schurath, U., and H.-J. Goede (1984), Temperature Dependence of the Reactions SO + O_3 (1) and SO + O_2 (2), in *Physico-Chemical Behaviour of Atmospheric Pollutants*, edited, pp. 227-239, Springer.
Seinfeld, J. H., and S. N. Pandis (2006), *Atmospheric Chemistry and Physics*, Wiley.
Sheng, J., D. K. Weisenstein, B. P. Luo, E. V. Rozanov, A. Stenke, J. G. Anet, H. G. Bingemer, and T. Peter (2015), Global atmospheric sulfur budget under volcanically quiescent conditions: Aerosol - chemistry - climate model predictions and validation, *Journal of Geophysical Research: Atmospheres*, *120*, 256 - 276, doi:10.1002/2014JD021985.
Singleton, D., and R. J. Cvetanović (1988), Evaluated chemical kinetic data for the reactions of atomic oxygen O (3P) with sulfur containing compounds, *Journal of physical and chemical reference data*, *17*(4), 1377-1437, doi:10.1063/1.555811.
Sorgo, M. D., A. Yarwood, O. Strausz, and H. Gunning (1965), The photolysis of carbon disulfide and carbon disulfide-oxygen mixtures, *Canadian Journal of Chemistry*, *43*(6), 1886-

1891.
Sunanda, K., A. Shastri, A. K. Das, and B. R. Sekhar (2015), Electronic states of carbon disulphide in the 5.5–11.8 eV region by VUV photo absorption spectroscopy, *Journal of Quantitative Spectroscopy and Radiative Transfer*, *151*, 76-87, doi:10.1016/j.jqsrt.2014.08.020.
Sze, N. D., and M. K. Ko (1980), Photochemistry of COS, CS_2, CH_3SCH_3 and H_2S: Implications for the atmospheric sulfur cycle, *Atmospheric Environment (1967)*, *14*(11), 1223-1239, doi:10.1016/0004-6981(80)90225-5.
Thalman, R., K. J. Zarzana, M. A. Tolbert, and R. Volkamer (2014), Rayleigh scattering cross-section measurements of nitrogen, argon, oxygen and air, *Journal of Quantitative Spectroscopy and Radiative Transfer*, *147*, 171-177.
Toon, O. B., J. F. Kasting, R. P. Turco, and M. S. Liu (1987), The sulfur cycle in the marine atmosphere, *Journal of Geophysical Research: Atmospheres*, *92*(D1), 943-963, doi:10.1029/JD092iD01p00943.
Torres, A., P. Maroulis, A. Goldberg, and A. Bandy (1980), Atmospheric OCS measurements on project GAMETAG, *Journal of Geophysical Research: Oceans*, *85*(C12), 7357-7360, doi:10.1029/JC085iC12p07357.
Turco, R., P. Hamill, O. Toon, R. Whitten, and C. Kiang (1979), A one-dimensional model describing aerosol formation and evolution in the stratosphere: I. Physical processes and mathematical analogs, *Journal of Atmospheric Sciences*, *36*(4), 699-717, doi:10.1175/1520-0469(1979)036%3C0699:AODMDA%3E2.0.CO;2.
Watts, S. F. (2000), The mass budgets of carbonyl sulfide, dimethyl sulfide, carbon disulfide and hydrogen sulfide, *Atmospheric Environment*, *34*(5), 761-779, doi:10.1016/S1352-2310(99)00342-8.
Weisenstein, D. K., G. K. Yue, M. K. Ko, N. D. Sze, J. M. Rodriguez, and C. J. Scott (1997), A two-dimensional model of sulfur species and aerosols, *Journal of Geophysical Research: Atmospheres*, *102*(D11), 13019-13035, doi:10.1029/97JD00901.
Whelan, M. E., S. T. Lennartz, T. E. Gimeno, R. Wehr, G. Wohlfahrt, Y. Wang, L. M. Kooijmans, T. W. Hilton, S. Belviso, and P. Peylin (2018), Reviews and syntheses: Carbonyl sulfide as a multi-scale tracer for carbon and water cycles, *Biogeosciences*, *15*(12), 3625-3657, doi:10.5194/bg-15-3625-2018.
Wine, P., W. Chameides, and A. Ravishankara (1981), Potential role of CS_2 photooxidation in tropospheric sulfur chemistry, *Geophys Res Lett*, *8*(5), 543-546, doi:10.1029/GL008i005p00543.
Wine, P., R. Shah, and A. Ravishankara (1980), Rate of reaction of hydroxyl with carbon disulfide, *The Journal of Physical Chemistry*, *84*(20), 2499-2503.
Wood, W. P., and J. Heicklen (1971), Photooxidation of carbon disulfide, *The Journal of Physical Chemistry*, *75*(7), 854-860, doi:10.1021/j100677a002.
Wordsworth, R., F. Forget, F. Selsis, J.-B. Madeleine, E. Millour, and V. Eymet (2010), Is Gliese 581d habitable? Some constraints from radiative-convective climate modeling, *Astronomy & Astrophysics*, *522*, A22, doi:10.1051/0004-6361/201015053.
Wu, C. R., and F. Chen (1998), Temperature-dependent photoabsorption cross sections of H2S in the 1600–2600 Å region, *Journal of Quantitative Spectroscopy and Radiative Transfer*, *60*(1), 17-23, doi:10.1016/S0022-4073(97)00163-5.

679 Wu, C. R., B. Yang, F. Chen, D. Judge, J. Caldwell, and L. Trafton (2000), Measurements of
680 high-, room-, and low-temperature photoabsorption cross sections of SO_2 in the 2080-to 2950-
681 Å region, with application to Io, *Icarus*, *145*(1), 289-296, doi:10.1006/icar.1999.6322.
682 Zeng, Z., M. Altarawneh, and B. Z. Dlugogorski (2017), Atmospheric oxidation of carbon
683 disulfide (CS_2), *Chemical Physics Letters*, *669*, 43-48, doi:10.1016/j.cplett.2016.11.058.
684 Zhang, L., Q. B. Li, Y. Gu, K. N. Liou, and B. Meland (2013), Dust vertical profile impact on
685 global radiative forcing estimation using a coupled chemical-transport–radiative-transfer
686 model, *Atmospheric Chemistry and Physics*, *13*(14), 7097-7114, doi:10.5194/acp-13-7097-
687 2013.
688 Zhang, L., and Q.-z. Qin (2000), Theoretical studies on $CS_2OH–O_2$: a possible intermediate in
689 the OH initiated oxidation of CS_2 by O_2, *Journal of Molecular Structure: THEOCHEM*, *531*(1-
690 3), 375-379, doi:10.1016/S0166-1280(00)00455-3.
691 Zhong, Q., H. Shen, X. Yun, Y. Chen, Y. a. Ren, H. Xu, G. Shen, W. Du, J. Meng, and W. Li
692 (2020), Global sulfur dioxide emissions and the driving forces, *Environmental science &*
693 *technology*, *54*(11), 6508-6517, doi:10.1021/acs.est.9b07696.

694